Supporting Information

Liu and Wilson 10.1073/pnas.1220560110

SI Methods

Fly Stocks. Flies were raised on standard cornmeal agar medium supplemented with potato food on a 12-h light/dark cycle at 25 °C. All experiments were performed on adult female flies 1–4 d after eclosion. The only exceptions were the experiments examining the effect of *GluClα* knockdown, where both control and RNAi flies were male. The genotypes used were as follows: Fig. 1 *B* and *C*, *OK371-Gal4/UAS-CD8:GFP*; Fig. 1 *D* and *E*, *pebbled-Gal4/+; UAS-nsyb:GFP/+*; Fig. 2, *OK371-Gal4/UAS-CD8:GFP*; Fig. 3 *A–D*, *GH146-Gal4,UAS-CD8:GFP*; Fig. 3 *D* and *E* and Fig. S1, *UAS-dicer2/Y;GH146-Gal4,UAS-CD8:GFP/+* (wild type) and *UAS-dicer2/Y;GH146-Gal4,UAS-CD8:GFP/ UAS-GluClα RNAi* (RNAi); Figs. 4 and 5, *OK371-Gal4,UAS-CD8:GFP/UAS-CD8:GFP;UAS-P2X2/+* (Glu-LN stimulation) and *UAS-CD8:GFP; UAS-P2X2/NP3056-Gal4* (GABA-LN stimulation); Fig. 6, *OK371-Gal4,UAS-CD8:GFP*; Fig. 7, *UAS-dicer2/Y;GH146-Gal4, UAS-CD8:GFP/+* (wild type) and *UAS-dicer2/Y;GH146-Gal4, UAS-CD8:GFP/UAS-GluClα RNAi* (RNAi); and Fig. S2, *GH146-Gal4,UAS-CD8:GFP*. Fly stocks were published as follows: *OK371-Gal4* (II) (1), *UAS-CD8:GFP* (II and III) (2), *pebbled-Gal4* (X) (3), *UAS-nsyb:GFP* (4), *GH146-Gal4* (II) (5), *UAS-P2X2* (III) (6), *NP3056-Gal4* (III) (7), *UAS-GluClα RNAi* (II) (8, 9), *UAS-dicer2* (X) (8). Stocks of *OK371-Gal4*, *UAS-CD8:GFP* (II and III), *UAS-nsyb:GFP*, and *UAS-dicer2* were obtained from the Bloomington *Drosophila* Stock Center. The *UAS-GluClα RNAi* insertion that we used in this study has been shown to substantially reduce *GluClα* RNAi levels in adult brain tissue (9), and we verified that it does not affect responses to iontophoresed GABA in these neurons (Fig. S1). However, it is difficult to completely exclude the possibility of off-target effects, given the lack of available alternative reagents for cross-validation. The *UAS-GluClα RNAi* insertion was obtained from the Vienna *Drosophila* RNAi Center (transformant ID 105754; sequence details available at http://stockcenter.vdrc.at).

Electrophysiological Recordings. In vivo whole-cell patch clamp recordings were performed essentially as described (10, 11). To perform recordings from Glu-LNs, the head was rotated 180° around the thin neck connective, so that the ventral side of the brain was facing upward and, therefore, accessible to visualization via the water-immersion objective above the preparation. The fly remained alive even when the head was rotated in this manner. The brain was perfused in external saline containing the following: 103 mM NaCl, 3 mM KCl, 5 mM *N*-Tris(hydroxymethyl) methyl-2-aminoethane-sulfonic acid, 8 mM trehalose, 10 mM glucose, 26 mM $NaHCO_3$, 1 mM NaH_2PO_4, 1.5 mM $CaCl_2$, and 4 mM $MgCl_2$ (osmolarity adjusted to 270–275 mOsm). The saline was bubbled with 95% O_2/5% CO_2 to pH 7.3. The internal solution for patch-clamp pipettes contained the following: 140 mM potassium aspartate, 10 mM Hepes, 1 mM EGTA, 4 mM MgATP, 0.5 mM Na_3GTP, 1 mM KCl, and 13 mM biocytin hydrazide. The pH of the internal solution was adjusted to 7.2, and the osmolarity was adjusted to ∼265 mOsm. In cases where antennal lobe projection neurons (PNs) and GABA-local neurons (LNs) were not labeled with GFP, they were identified based on the location and size of their somata, along with their distinctive intrinsic electrophysiological properties (11). Specifically, to record from PNs, we targeted our electrodes to the cluster of cell bodies immediately anterodorsal to the antennal lobe neuropil, which contains a pure population of uniglomerular PNs (12, 13). We confirmed that all these cells had small-amplitude action potentials (<12 mV), which is diagnostic of PNs (11). We also filled a subset of these cells with biocytin and verified that they were PNs based on their morphology. To record from GABA-LNs, we targeted our electrodes to the cluster of cell bodies lateral to the antennal lobe neuropil. This cluster contains both PNs and GABA-LNs (12, 13), but GABA-LNs are easily identifiable on the basis of their large action potentials (>24 mV), again as confirmed by biocytin fills (10, 11, 14). Glu-LN somata are located ventral to the antennal lobe, and so are in a distinctly different location from PN and GABA-LN somata. Glu-LN somata were always targeted for recording based on GFP expression (in *OK371-Gal4,UAS-CD8:GFP* flies), and in a subset of recordings, we used biocytin fills to verify that the GFP^+ cells we recorded from in this cluster were always antennal lobe LNs. Recordings were performed with an Axopatch 200B amplifier (Axon Instruments). Recorded voltages were low-pass filtered at 5 kHz and digitized at 10 kHz.

Odor Stimulation. Odors used were diluted 100-fold in paraffin oil and delivered via a custom-built olfactometer, which further dilutes the headspace of the odor vial 10-fold in air (15). Odor was delivered at a flow rate of 2.2 mL/min. Odor stimuli were applied for 2 s every 30 s, with five or six trials per stimulus. In one experiment, we observed odor-evoked firing rates that varied more than twofold over the course of the experiment, and we excluded this experiment from further analysis.

Histochemistry. In some experiments, the morphology of the recorded neurons was visualized after recording by incubating the brain with a fluorescent conjugate of streptavidin, as published (11). Immunohistochemistry was performed as described (10, 11). Primary antibodies were obtained from the following sources (with dilutions in parentheses): mouse nc82 from the Developmental Studies Hybridoma Bank (1:20), rat anti-CD8 from Invitrogen (1:200), rabbit anti-VGluT from A. DiAntonio (Washington University, St. Louis) (1:500; ref. 16), and rabbit anti-VGAT from D. E. Krantz (University of California, Los Angeles, CA) (1:200; ref. 17). Secondary antibodies (Invitrogen) were used at 1:250. To reconstruct neuronal morphology from biocytin fills, we hand-traced the skeletonized morphology with the Simple Neurite Tracer plugin in Fiji, using the Fill Out command to automatically generate a 3D volume, which we subsequently converted to a *z*-projection.

Glutamate and GABA Iontophoresis. For glutamate iontophoresis, a high-resistance sharp pulled glass pipette was filled with a solution of 1 M monosodium glutamate in water (pH 8). The pipette was placed in the antennal lobe neuropil, and glutamate was ejected by using a 10- to 20-ms negative current pulse applied with an iontophoresis current generator gated by a voltage pulse (Model 260; World Precision Instruments). A constant positive backing current was applied to retain glutamate in the pipette between ejections. The magnitude of the iontophoresis response depends on the placement of the pipette and the ejection current magnitude and duration, and these variables were adjusted in each experiment to ensure that the ejection artifact was small. (The artifact is visible as a downward deflection and flips symmetrically to become an upward deflection when the ejection pulse is inverted.) Because these adjustments are necessarily subjective, in the experiments comparing two genotypes (Fig. 3 *E* and *F*), the experimenter was blinded to genotype. For GABA iontophoresis, the glass pipette was filled with 250 mM GABA in water (pH 4.3). GABA was ejected by using a 20-ms positive pulse, and a negative backing current was applied to retain

GABA in the pipette between ejections. Tetrodotoxin (1 μM) was added to the bath in all iontophoresis experiments to block network activity.

Stimulation of LNs with ATP/P2X2. We used ATP/P2X2 to stimulate glutamatergic neurons because we found that expression of channelrhodopsin-2 under control of the *OK371-Gal4* driver produced lethality, likely due to basal activity of channelrhodopsin-2 in motorneurons. In our experiments using the ATP/P2X2 system (6), the ATP ejection pipette was filled with 10 mM MgATP in water and placed near the edge of the antennal lobe neuropil at the base of the ipsilateral antennal nerve (for Glu-LN activation), or at the dorsolateral edge of the antennal lobe neuropil (for GABA-LN activation). The ATP solution was pressure ejected for 10 ms at 6 psi by using a pneumatic device gated by a voltage pulse (PV820; World Precision Instruments). As a negative control, we recorded from Glu-LNs that lacked P2X2 expression (genotype *OK371-Gal4,UAS-CD8:GFP*) and confirmed that they were not depolarized by ATP. As an additional negative control, we also recorded from PNs and GABA-LNs in flies lacking the Gal4 driver (genotype *UAS-CD8:GFP*; *UAS-P2X2*) and confirmed that ATP ejection elicited a negligible response in these cells. However, if the ejection duration was prolonged beyond 10 ms, or if the pipette was buried in the antennal lobe neuropil, we observed a depolarization evoked by ATP pressure ejection in these control recordings.

Paired Recordings. Paired recordings were performed in an ex vivo preparation where the brain was removed from the head and immobilized on a coverslip. To target Glu-LNs in the paired recordings, we expressed GFP under the control of the *OK371-Gal4* driver. PNs and GABA-LNs were unlabeled but could be identified based on their soma location, soma size, and spike shape. The presynaptic cell was stimulated by injecting a 500-ms step of depolarizing current. The size of the step was adjusted to achieve depolarizations >30 mV in the stimulated cell. Current injections were repeated every 6 s for 30–60 trials. The response of the unstimulated cell was low-pass filtered at 50 Hz and averaged across trials. A pair was defined as connected if the response of the unstimulated cell was >0.3 mV. In a few cases, we defined a pair as connected even though the response was <0.3 mV, because the response was abolished by a neurotransmitter receptor antagonist (picrotoxin, CGP54626, or mecamylamine). In some pairs, we saw evidence of weak ephaptic coupling. These responses were small (typically <0.2 mV in the unstimulated cell) and had a latency and shape that was very similar to the voltage deflection in the stimulated cell, but in the opposite direction. They were not abolished by tetrodotoxin (1 μM).

Electrical Stimulation of Olfactory Receptor Neuron Axons. Electrical stimulation of the antennal nerve (in Fig. S2) was performed essentially as described (18). The ipsilateral antennal nerve was severed and drawn into a saline-filled suction electrode. A pair of 50-μs current pulses, 25 ms apart, was delivered to the nerve by using a current isolator (A.M.P.I.). We discarded trials in which there were unclamped spikes. We also discarded trials in which there were failures in either $EPSC_1$ or $EPSC_2$ (defined as events with an amplitude < 20% of the trial-averaged amplitude for that EPSC). Unitary EPSCs at this synapse are generally highly reliable in their trial-to-trial amplitudes, and so we interpret these failures as failures of axon recruitment, not failures of synaptic vesicle release. Consistent with this interpretation, we could sometimes obtain a more reliable recording by releasing and then reinserting the nerve into the suction electrode. Because of occasional large fluctuations in EPSC amplitude (likely due to fluctuating recruitment of axons), we only analyzed paired-pulse ratios over a run of trials where recruitment was stable. Specifically, paired-pulse ratios were measured over the maximum window of consecutive trials where the trial-to-trial coefficient of variation in $EPSC_1$ amplitude was less than 30%, where the minimum number of consecutive trials must be at least six. In these experiments, the iontophoretic ejection current began 400 ms before $EPSC_1$ and lasted 50 ms. This protocol ensured that the evoked EPSCs fell within the steady state of the postsynaptic outward current evoked by glutamate. The postsynaptic outward current evoked by glutamate iontophoresis was on average 6 pA, which was 22% of the average magnitude of $EPSC_1$ (27 pA). Current traces were low-pass filtered at 1 kHz before digitization at 10 kHz.

1. Mahr A, Aberle H (2006) The expression pattern of the Drosophila vesicular glutamate transporter: A marker protein for motoneurons and glutamatergic centers in the brain. *Gene Expr Patterns* 6(3):299–309.
2. Lee T, Luo L (1999) Mosaic analysis with a repressible cell marker for studies of gene function in neuronal morphogenesis. *Neuron* 22(3):451–461.
3. Sweeney LB, et al. (2007) Temporal target restriction of olfactory receptor neurons by Semaphorin-1a/PlexinA-mediated axon-axon interactions. *Neuron* 53(2):185–200.
4. Zhang YQ, Rodesch CK, Broadie K (2002) Living synaptic vesicle marker: Synaptotagmin-GFP. *Genesis* 34(1-2):142–145.
5. Stocker RF, Heimbeck G, Gendre N, de Belle JS (1997) Neuroblast ablation in Drosophila P[GAL4] lines reveals origins of olfactory interneurons. *J Neurobiol* 32(5): 443–456.
6. Lima SQ, Miesenböck G (2005) Remote control of behavior through genetically targeted photostimulation of neurons. *Cell* 121(1):141–152.
7. Chou YH, et al. (2010) Diversity and wiring variability of olfactory local interneurons in the Drosophila antennal lobe. *Nat Neurosci* 13(4):439–449.
8. Dietzl G, et al. (2007) A genome-wide transgenic RNAi library for conditional gene inactivation in Drosophila. *Nature* 448(7150):151–156.
9. Collins B, Kane EA, Reeves DC, Akabas MH, Blau J (2012) Balance of activity between LN(v)s and glutamatergic dorsal clock neurons promotes robust circadian rhythms in Drosophila. *Neuron* 74(4):706–718.
10. Wilson RI, Laurent G (2005) Role of GABAergic inhibition in shaping odor-evoked spatiotemporal patterns in the Drosophila antennal lobe. *J Neurosci* 25(40): 9069–9079.
11. Wilson RI, Turner GC, Laurent G (2004) Transformation of olfactory representations in the Drosophila antennal lobe. *Science* 303(5656):366–370.
12. Jefferis GS, Marin EC, Stocker RF, Luo L (2001) Target neuron prespecification in the olfactory map of Drosophila. *Nature* 414(6860):204–208.
13. Lai SL, Awasaki T, Ito K, Lee T (2008) Clonal analysis of Drosophila antennal lobe neurons: diverse neuronal architectures in the lateral neuroblast lineage. *Development* 135(17):2883–2893.
14. Yaksi E, Wilson RI (2010) Electrical coupling between olfactory glomeruli. *Neuron* 67(6):1034–1047.
15. Olsen SR, Bhandawat V, Wilson RI (2007) Excitatory interactions between olfactory processing channels in the Drosophila antennal lobe. *Neuron* 54(1):89–103.
16. Daniels RW, Gelfand MV, Collins CA, DiAntonio A (2008) Visualizing glutamatergic cell bodies and synapses in Drosophila larval and adult CNS. *J Comp Neurol* 508(1): 131–152.
17. Fei H, et al. (2010) Mutation of the Drosophila vesicular GABA transporter disrupts visual figure detection. *J Exp Biol* 213(Pt 10):1717–1730.
18. Kazama H, Wilson RI (2008) Homeostatic matching and nonlinear amplification at identified central synapses. *Neuron* 58(3):401–413.

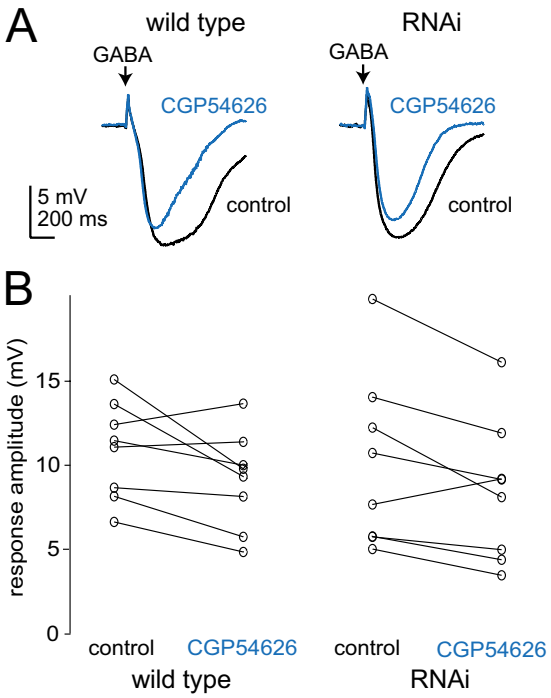

Fig. S1. *GluClα* knockdown does not affect PN responses to GABA. (*A*) Whole-cell recordings from an antennal lobe PN in a wild-type fly (*Left*) and a fly where the *GluClα* RNAi construct is expressed specifically in PNs (*Right*). A pulse of GABA in the antennal lobe neuropil (arrow) hyperpolarizes the PN in both cases. CGP54626 (50 μM) blocks the $GABA_B$ component of these responses, and what remains is the $GABA_A$ component (1). Note that the responses to GABA are similar in the two cells, as is the fractional block by CGP54626. (*B*) Group data showing responses to GABA iontophoresis in all experiments, before and after adding CGP54626. The percent inhibition by CGP54626 is not significantly different in the control and RNAi genotype ($P = 0.97$, student's *t* test). This result demonstrates that the RNAi construct is specific for *GluClα* and does not affect GABA receptors.

1. Wilson RI, Laurent G (2005) Role of GABAergic inhibition in shaping odor-evoked spatiotemporal patterns in the Drosophila antennal lobe. *J Neurosci* 25(40):9069–9079.

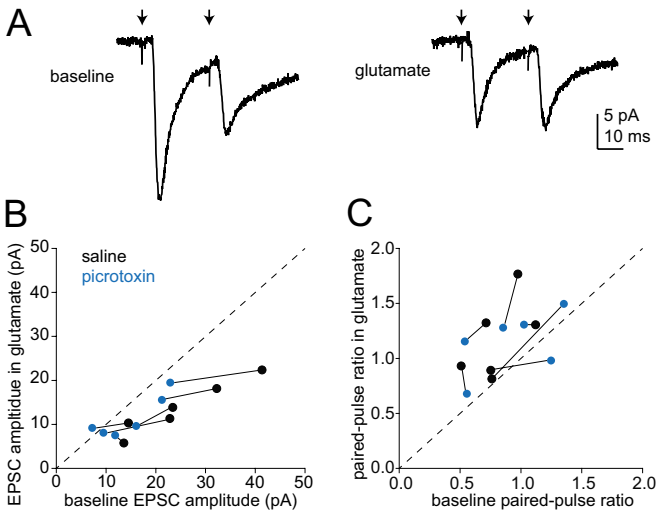

Fig. S2. Glutamate inhibits olfactory receptor neuron (ORN)-to-PN synapses. (*A*) A voltage-clamp recording from a PN shows EPSCs evoked by stimulation of ORN axons in the antennal nerve with a pair of electrical pulses (arrows). Glutamate iontophoresis inhibits EPSC amplitude. Glutamate also increases the relative size of EPSC2 to EPSC1, defined as the paired-pulse ratio (PPR = EPSC2/EPSC1). Traces are averages of 14 trials. (*B*) Summary of the effects of glutamate on EPSC1, where each symbol is a different experiment. Glutamate significantly inhibits EPSC1 amplitude ($P < 0.005$, two-way repeated-measures ANOVA, $n = 6$). The magnitude of inhibition by glutamate is significantly reduced by 100 μM picrotoxin (blue symbols, $P < 0.01$, two-way repeated-measures ANOVA), implying that GluCl contributes to this inhibition. Lines connect symbols corresponding to the same experiment. (*C*) Summary of the effects of glutamate on the paired-pulse ratio. Glutamate significantly increases PPR ($P < 0.05$, $n = 6$). An increase in PPR is classically associated with a decrease in presynaptic neurotransmitter release (1). However, picrotoxin does not significantly change the effect of glutamate on PPR ($P = 0.19$, two-way repeated-measures ANOVA). This result may reflect incomplete blockade of glutamate-gated chloride channels by picrotoxin (Fig. 3*D*) or an additional contribution to presynaptic inhibition from other glutamate receptors (e.g., a metabotropic glutamate receptor). In sum, these data show that the effects of iontophoretic glutamate on ORN-to-PN synapses are very similar to the effects of iontophoretic GABA (2, 3). This effect appears to be at least partly mediated by glutamate-gated chloride conductances, although metabotropic glutamate receptors may also contribute to presynaptic inhibition. Interestingly, GABAergic inhibition of neurotransmitter release from ORNs also appears to be mediated by both ionotropic and metabotropic GABA receptors (2).

1. Zucker RS, Regehr WG (2002) Short-term synaptic plasticity. *Annu Rev Physiol* 64:355–405.
2. Olsen SR, Wilson RI (2008) Lateral presynaptic inhibition mediates gain control in an olfactory circuit. *Nature* 452(7190):956–960.
3. Root CM, et al. (2008) A presynaptic gain control mechanism fine-tunes olfactory behavior. *Neuron* 59(2):311–321.